HOKKAIDO UNIVERSITY

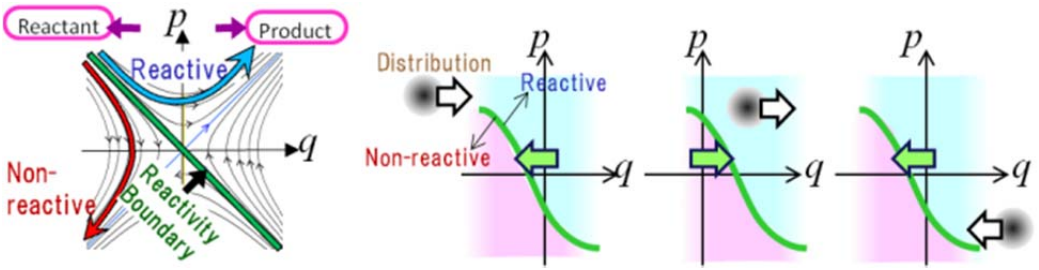
Title	Laser Control of Chemical Reactions by Phase Space Structures
Author(s)	Kawai, Shinnosuke; Komatsuzaki, Tamiki
Citation	Bulletin of the Chemical Society of Japan, 85(8), 854-861 https://doi.org/10.1246/bcsj.20120085
Issue Date	2012-08
Doc URL	https://hdl.handle.net/2115/53050
Type	journal article
File Information	BCSJ85-8_854-861.pdf

Hokkaido University Collection of Scholarly and Academic Papers : HUSCAP

Laser Control of Chemical Reactions by Phase Space Structures

Shinnosuke Kawai*, Tamiki Komatsuzaki
Molecule & Life Nonlinear Sciences Laboratory,
Research Institute for Electronic Science, Hokkaido University,
Kita 20 Nishi 10, Kita-ku, Sapporo 001-0020, Japan
E-mail: skawai@es.hokudai.ac.jp

Chemical reactions can be controlled by applying a laser pulse designed in such a way that increases the population in the reactive region of the phase space.



Synopsis

The question of what initial conditions or what kinds of laser fields can effectively carry a system to the desired products is one of the most intriguing subjects in chemistry. In this paper, a scheme for designing a laser field to guide a chemical reaction system into the product is presented on the basis of the phase space structure of the reaction with an illustrative simple example. The method exploits recent findings [Kawai *et al.*, *J. Chem. Phys.* **2011**, *134*, 024317] that have revealed the existence of a rigorous reactivity boundary separating the reactive and non-reactive trajectories in the phase space (more precisely, the semi-classical phase space representation of the quantum system). Referring to the time propagation of the system, the method designs an electric field that actively shifts this reactivity boundary so that it catches more the system in the reactant and releases the system in the product. The success of this scheme for designing of the field gives a further support to the interpretation for the laser control of chemical reactions.

Controlling chemical reactions is one of the major goals of the fundamental study of chemistry. In the last decades there have been extensive studies on the controllability of reactions by using laser fields[1–5] in both theoretical formulations[6–15] and experimental demonstrations.[16–18] Theories for calculating the optimal pulse shape designed for obtaining the target state (desired products of chemical reactions) are called Optimal Control Theory (OCT). The basic formulation of OCT is done by first setting up a functional of the laser field $F(t)$, time-dependent electric field, to measure the "success" of control and then maximizing it with respect to $F(t)$.[6] The functional, called the *cost*, usually includes the population in the target quantum state at the final time $t_{\mathrm{fin}} > 0$, where $t = 0$ is the initial time, and penalty factors to limit the energy of the pulse. The penalty factor can be proportional to the integration of the laser power $|F(t)|^2$ over time t, or be in the form of the Lagrange multiplier. It is also suggested to introduce a time-dependent penalty factor[10] to make the laser power zero at the initial ($t = 0$) and final ($t = t_{\mathrm{fin}}$) times and exert the pulse only in the middle times. One can also put frequency constraints[11,12] in order to make a laser pulse containing only the frequencies available in specific experimental apparatus and to exploit pre-knowledge about relative importance of each frequency to accelerate the convergence. There is a mathematical proof that the optimization of the cost functional converges monotonically[7,8] in the absence of frequency constraints. When the frequency constraints are used, one needs an additional technique to ensure the monotonic convergence.[13] An extension of the theory into nonlinear interaction between the system and the electric field has also been given.[13] The global OCT performs iterative calculations to improve the pulse field until it converges. Each iteration step needs a numerical solution of the Schrödinger equation and therefore requires significant computational power. On the other hand, the local OCT[14] optimizes the field at each time step so that only one time propagation is needed. Finally, geometric analysis has been provided[15] about the landscape of the control. The electric field $F(t)$, being a function of time t in $0 \le t \le t_{\mathrm{fin}}$, forms an infinite dimensional space. The optimal field is given by a global minimum of the cost functional in this infinite dimensional space. For an N-level quantum system, the analysis of the curvatures of the landscape found that at the global minimum, the cost functional is minimum along at most N^2 directions and the curvature is zero along the other directions.

After the optimal field is obtained by these algorithms, it can be asked, from the viewpoint of fundamental study, why the particular pulse shape leads to the target state. It is desired to obtain basic physical insights on what is taking place in the system under the optimally designed pulse output from the "black-box" numerical algorithm. In previous

papers,[19,20] we have applied a recently developed theory of the saddle region dynamics[21–44] to laser-controlled reaction systems. A saddle point is a point on the potential energy surface where the potential energy is maximum along one direction corresponding to the reaction and minimum along the others. Such a point is often found between the reactant and product regions, and the saddle region dynamics plays a primary role in determining whether the system goes through the saddle to become products or not. Studies of classical dynamics[21,22,25–44] in the saddle region and their quantum extension[20,23,24,45,46] found, under certain conditions, robust existence of a "reactivity boundary" which lies in the phase space and separates the phase space points going to the product region and those going to the reactant region. In the context of the quantum dynamics, the phase space and geometric objects in it should be understood in terms of the Wigner distribution and the Weyl representation which have one-to-one correspondence to the quantum mechanical operators.[45,47]

By extending the above mentioned theories of saddle region dynamics into systems under time-dependent laser fields, it has been enabled to extract the time-dependent reactivity boundary in these systems. The reaction boundary was found to move with time by the time-dependence of the laser field, so that the boundary "catches" the system excited in the reactant and "releases" it into the product, resulting in an increase of the reaction probability. It is thus enabled to give an *interpretation* of the controlled reaction *after* the optimal field is obtained. In this paper, we demonstrate a *construction of the field* on the basis of this physical interpretation. Showing that the physical interpretation is indeed capable of giving the control field to guide the reaction, the result will give further support to the validity of the physical understanding of the previous studies. We first review briefly the findings of the previous studies of the saddle region dynamics, and then present a scheme to construct an electric field that is consistent with the physical interpretation obtained by these theories. A numerical demonstration will be given for a simple one-dimensional model.

Theoretical

Review of previous theories

In this section we explain the motion taking place in the vicinity of the saddle point. We treat the dynamics to the lowest approximation, one-dimensional parabolic barrier. Extension to multi-dimensional systems with anharmonicity and couplings among the degrees of freedom can be found in many books[21,22] and papers.[19,20,23–30,32,44,45,47] In the vicinity of the saddle point, the Hamiltonian without the laser field can be approximated by

$$H(q,p) = \frac{p^2}{2} - \frac{\lambda^2}{2} q^2, \tag{1}$$

where q is the position coordinate of the system and p its conjugate momentum. We take the origin (q = 0) of the coordinate system at the saddle point, where the curvature of the potential is $-\lambda^2/2$. The sign of q is such that $q < 0$ corresponds to the reactant region and $q > 0$ to the product. In this case, one can easily assign the reactivity of the system: If the total energy H is higher than the potential energy at the saddle point [taken as zero in Eq.(1)], then the system can go over the barrier from the reactant to the product side or vice versa. If the total energy H is below zero, then the system will be reflected back and the reaction will not occur.

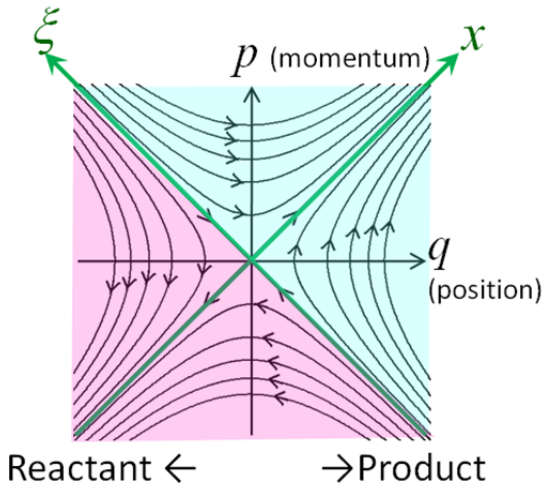


Fig. 1 Phase space flow in the saddle region, for the case of one-dimensional harmonic system without laser field. The line x = 0 separates the destination of trajectories; trajectories with $x > 0$ (colored by blue) go to the the product side, while those with $x < 0$ (red) go to the reactant side.

The classical trajectories given by the Hamiltonian of Eq. (1) are depicted in Fig. 1. Because of the conservation of energy, they draw hyperbolas given by $H(q,p) = \frac{p^2}{2} - \frac{\lambda^2}{2} q^2 = \text{const.}$

The following set of variables is often useful in theoretical investigations:

$$x = \frac{\lambda q + p}{\sqrt{2\lambda}}, \qquad \xi = \frac{p - \lambda q}{\sqrt{2\lambda}}. \tag{2}$$

These variables (x, ξ) define a skewed coordinate system in the phase space as in Fig. 1, and the two straight asymptotic lines of the hyperbolas are given by $x = 0$ and $\xi = 0$. In these coordinates, the Hamiltonian can be written as

$$H = \lambda x \xi, \tag{3}$$

and their equations of motion are given by

$$\frac{\mathrm{d}x}{\mathrm{d}t} = \lambda x,$$
$$\frac{\mathrm{d}\xi}{\mathrm{d}t} = -\lambda \xi. \tag{4}$$

The trajectories with $x > 0$ and $\xi > 0$ are "forward reactive" trajectories because they climb up from the reactant region, overcome the barrier, and go down to the product region (*i.e.*, the reaction occurs). On the other hand, the trajectories with $x < 0$ and $\xi > 0$ are "forward non-reactive" trajectories because they start in the reactant region, but are reflected by the barrier, and go back into the reactant region. The trajectories with $x < 0$ and $\xi < 0$ are "backward reactive" trajectories, because they climb up from the product region and go down the barrier to the reactant region (*i.e.*, the backward reaction). Similarly, the trajectories with $x > 0$ and $\xi < 0$ are "backward non-reactive" trajectories. Note that the sign of x determines the fate of the system, that is, if x is positive (negative), the trajectory will go to the product (reactant, resp.) side, without mattering where it initially was. The set $\{x = 0\}$, *i.e.*, the ξ-axis, thus divides all the climbing trajectories into two disjoint sets: ones going to the product and the others going to the reactant. Once we know the sign of x, we can tell the fate of the reaction without further observing the trajectory. In addition, once the system is located *on* the dividing surface $\{x = 0\}$, it stays there perpetually (*i.e.*, the set $\{x = 0\}$ forms an invariant manifold in the phase space).

While the destination region of a trajectory is determined by the sign of x in classical mechanics, its quantum counterpart can be found by using the Wigner distribution.[48,49] For a quantum state $|\psi\rangle$, the Wigner distribution is defined as

$$\rho_\psi(q,p) = (2\pi\hbar)^{-1} \int \left\langle q - \tfrac{s}{2} \middle| \psi \right\rangle \left\langle \psi \middle| q + \tfrac{s}{2} \right\rangle \exp\left(\frac{\mathrm{i}sp}{\hbar}\right) \mathrm{d}s. \tag{5}$$

It is shown[20] that, without any "(semi-)classical approximation", the quantum mechanical reaction probability for the parabolic barrier is given by integrating the Wigner distribution in

the region $x > 0$:

$$P_{\text{reaction}} = \int \rho_{\psi}(q,p)\Theta(x)\mathrm{d}q\mathrm{d}p, \tag{6}$$

where the step function $\Theta(x)$ is 1 if $x > 0$ and 0 if $x < 0$.

Now we include the effect of the external field. The Hamiltonian is given by

$$H(q,p) = \frac{p^2}{2} - \frac{\lambda^2}{2}q^2 + \mu(q)F(t), \tag{7}$$

where $\mu(q)$ is the dipole moment and $F(t)$ is the electric field. We consider here only the lowest order of the expansion of μ:

$$\mu(q) = \mu_0 + \mu_1 q + \cdots. \tag{8}$$

The treatment of the higher order terms in the expansion, as well as the nonlinear dependence of the Hamiltonian on $F(t)$, can again be found in the previous works.[19,20] The equations of motion for x and ξ now read

$$\begin{aligned} \frac{\mathrm{d}x}{\mathrm{d}t} &= \lambda x - \frac{1}{\sqrt{2\lambda}}\mu_1 F(t), \\ \frac{\mathrm{d}\xi}{\mathrm{d}t} &= -\lambda\xi - \frac{1}{\sqrt{2\lambda}}\mu_1 F(t). \end{aligned} \tag{9}$$

If we define the following time-dependent functions

$$\begin{aligned} x^{\ddagger}(t) &\stackrel{\text{def}}{=} \frac{1}{\sqrt{2\lambda}}\mu_1 \int_t^{+\infty} \exp(\lambda(t-\tau))F(\tau)\mathrm{d}\tau, \\ \xi^{\ddagger}(t) &\stackrel{\text{def}}{=} -\frac{1}{\sqrt{2\lambda}}\mu_1 \int_{-\infty}^{t} \exp(-\lambda(t-\tau))F(\tau)\mathrm{d}\tau, \end{aligned} \tag{10}$$

and perform a coordinate transformation $(x, \xi) \rightarrow (\Delta x, \Delta\xi)$ by

$$\begin{aligned} x &= x^{\ddagger}(t) + \Delta x, \\ \xi &= \xi^{\ddagger}(t) + \Delta\xi, \end{aligned} \tag{11}$$

the equations of motion [Eq.(9)] are transformed to the following:

$$\frac{\mathrm{d}}{\mathrm{d}t}\Delta x = \lambda\Delta x,$$

$$\frac{\mathrm{d}}{\mathrm{d}t}\Delta\xi = -\lambda\Delta\xi.$$

(12)

Since Eq. (12) has the same form with Eq. (4), we can draw the same picture as Fig. 1 with the name of axes changed to (Δx, $\Delta\xi$). The destination of the trajectory can now be told by the sign of Δx. In the plot with the original coordinate (x, ξ), the reactivity boundaries are now given by $x = x^{\ddagger}(t)$ and $\xi = \xi^{\ddagger}(t)$ rather than $x = 0$ and $\xi = 0$. In other words, the reactivity boundaries are shifted by the amount of $(x^{\ddagger}(t),\ \xi^{\ddagger}(t))$, since the coordinate transformation Eq. (11) is a time-dependent origin shift. In the (q, p)-coordinates, the amount of the origin shift is expressed by

$$q^{\ddagger}(t) = \sqrt{\frac{1}{2\lambda}}\left(x^{\ddagger}(t) - \xi^{\ddagger}(t)\right),$$

$$p^{\ddagger}(t) = \sqrt{\frac{\lambda}{2}}\left(x^{\ddagger}(t) + \xi^{\ddagger}(t)\right),$$

(13)

corresponding to Eq. (2). The shift of the reactivity boundaries caused by the laser field is schematically drawn in Fig. 2 (a).

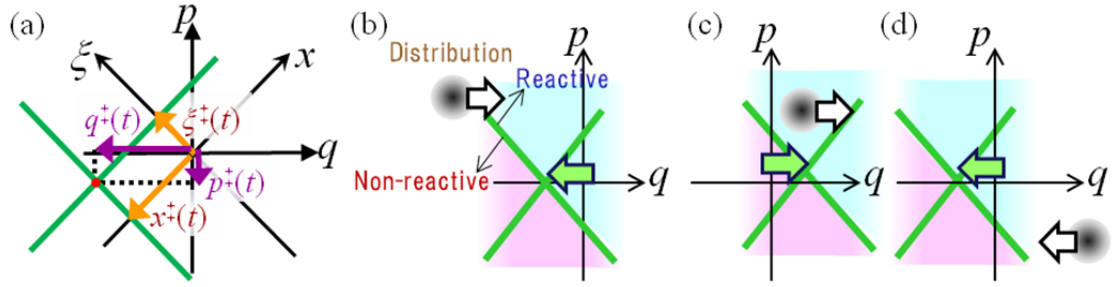


Fig. 2 Schematic representation of (a) shift of the reactivity boudaries, and (b)–(d) the catch-and-release mechanism of reaction control . The laser field shifts the reactivity boundary by the amount $(q^{\ddagger}(t),\ p^{\ddagger}(t))$. Under the effect of the designed field for control, the boundaries shift toward the distribution in the reactant region to catch the system into the reactive region when the system is dominantly distributed in the reactant region (b). The boundaries then push the system to the right and release it into the product region (c). When the system is on the product side and heading to the left, the boundaries are shifted to the left to prohibit the system from entering the backward-reactive region (d).

In the previous work,[20] we calculated the reactivity boundaries under the effect of the electric field obtained by the OCT. It was found that the reactivity boundaries are moved by the field accordingly to the movement of the system, resulting in the enhancement of the reaction: When the Wigner distribution of the system is predominantly located in the reactant region and moving toward the right direction (toward the product side), the boundaries move, by the effect of the control field, toward the left to increase the population included in the reactive region [Fig. 2 (b)]. Once the system has entered into the forward-reactive region, the boundaries move toward the right to guide the system into the product side [Fig. 2 (c)]. In this paper we call this movement of the boundaries "catch-and-release mechanism" because the boundaries go to catch the system in the reactant region and then release it into the product side.

Algorithm for Designing Pulse Shape Using the Catch-and-release Mechanism

Here we consider a control method based on the interpretation of control mechanism found in the previous work. From the findings summarized in the previous section, we wish the boundaries to shift toward the reactant side for catching the system lying on the reactant side and heading for the product side, and then to move toward the product side for guiding the system to the product and releasing it. In addition, when the system is on the product side and moving toward the reactant side, we wish to decrease the probability of the backward reaction, by shifting the boundaries toward the reactant region [Fig. 2 (d)]

According to the above requirement, we set the shift $q^{\ddagger}(t)$ proportional to the average of the product of q and p: That is, when the system is on the reactant side ($q < 0$) with positive momentum $p > 0$, the reactivity boundaries $q^{\ddagger}(t)$ shift in negative direction toward the reactant side to catch the system [Fig. 2 (b)]. On the other hand, once the system arrives in the product side with positive momentum ($q > 0, p > 0$), $q^{\ddagger}(t)$ shifts in positive direction to put the system into the product region [Fig. 2 (c)]. Likewise, when the system has negative momentum ($p < 0$) on the product side ($q > 0$) and tries to go back to the reactant, $q^{\ddagger}(t)$ shifts in negative direction to prevent the system from returning to the reactant side [Fig. 2 (d)]. Thus we set

$$q^{\ddagger}(t) = \alpha' \left\langle \psi(t) \middle| \frac{\hat{q}\hat{p} + \hat{p}\hat{q}}{2} \middle| \psi(t) \right\rangle, \tag{14}$$

with some proportionality constant $\alpha' > 0$. Due to the non-commutativity of $\hat{q}$ and $\hat{p}$, we have put the average of $\hat{q}\hat{p}$ and $\hat{p}\hat{q}$ to make a Hermitian operator.

From Eqs. (10) and (13), we can solve Eq. (14) in terms of the electric field $F(t)$:

$$F(t) = \alpha\left(\lambda^2 - \frac{\mathrm{d}^2}{\mathrm{d}t^2}\right)\left\langle\psi(t)\middle|\frac{\hat{q}\hat{p}+\hat{p}\hat{q}}{2}\middle|\psi(t)\right\rangle, \tag{15}$$

where $\alpha = \alpha'/\mu_1$. The detailed derivation of Eq. (15) is given in the appendix. This equation, together with the Schrödinger equation

$$\mathrm{i}\hbar\frac{\partial}{\partial t}\psi(t) = \hat{H}(t)\psi(t), \tag{16}$$

gives a simultaneous time evolution equation for $\psi(t)$ and $F(t)$.

Eq. (15) contains the second-order time derivative of $\psi(t)$, whose time propagation depends on the electric field $F(t)$ through Eq. (16). We adopt the following locally iterative method to solve these equations for $F(t)$: We set up a small time window (*e.g.* a few propagation steps) and propagate the system for this interval according to Eq. (16) with zero field. Then we obtain the right hand side of Eq. (15), which in turn is inserted into Eq. (16) and time propagation in the same time interval is again performed with the new field. This procedure is repeated until convergence. In the next section we demonstrate numerical results obtained with the method presented above by using a model system, and check its validity for control.

Results and Discussion

The model system we use here for demonstration is a one-dimensional system with a dipole couping to the laser field, which was regarded as mimicking the isomerization of trimethylenimine.[14] The Hamiltonian is given by

$$H = \frac{p^2}{2m} + V(q) + F(t)\mu(q), \tag{17}$$

with the effective mass m = 99.33 amu, the potential energy

$$V(q) = -\frac{m\lambda^2}{2}q^2 + a_3q^3 + a_4q^4, \tag{18}$$

$m\lambda^2/2 = 3.79\ \mathrm{cm^{-1}Å^{-2}}$, $a_3 = 1.59\ \mathrm{cm^{-1}Å^{-3}}$, $a_4 = 9.22\ \mathrm{cm^{-1}Å^{-4}}$, the time-dependent electric field $F(t)$, and the dipole moment

$$\mu(q) = \mu_1 q,$$

(19)

with $\mu_1 = 0.301e$. The potential energy, energy eigenvalues and eigenfunctions without the electric field are shown in Fig. 3. Throughout the numerical calculations, we use the sinc-function discrete variable representation of Colbert and Miller,[50] where the interval of $q \in [-0.4\ \text{Å}, 0.4\ \text{Å}]$ is divided into 80 equally-spaced grid points. Numerical results for the transition energies and the transition moments are shown in Tables 1 and 2.

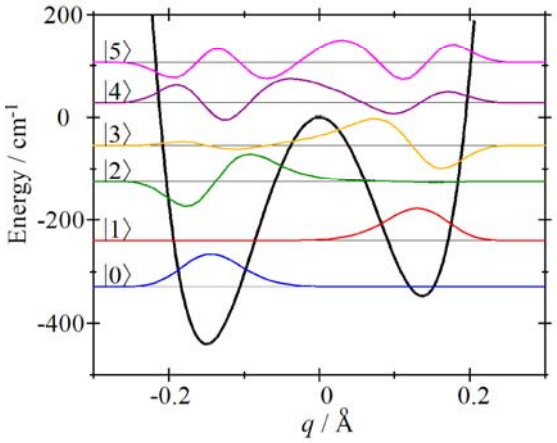


Fig. 3 Potential energy, energy eigenvalues and eigenfunctions of the model system.

i	j	N=10	N=20	N=40	N=80	N=200
0	1	121.013	88.612	88.378	88.378	88.378
0	2	231.051	202.544	202.787	202.787	202.787
0	3	255.828	273.256	273.741	273.741	273.741
0	4	475.767	358.265	356.574	356.574	356.574
0	5	1102.587	437.000	435.797	435.797	435.797
1	2	110.038	113.933	114.409	114.409	114.409
1	3	134.815	184.644	185.363	185.363	185.363
1	4	354.754	269.653	268.195	268.195	268.195
1	5	981.574	348.388	347.419	347.419	347.419
2	3	24.777	70.712	70.954	70.954	70.954
2	4	244.716	155.721	153.786	153.786	153.786
2	5	871.536	234.456	233.010	233.010	233.010
3	4	219.939	85.009	82.832	82.832	82.832
3	5	846.759	163.744	162.056	162.056	162.056
4	5	626.820	78.735	79.224	79.224	79.224

TABLE 1: Numerical values of the transition frequency $E_j - E_i$ in cm^{-1}, where E_i and E_j are the eigenenergies of the states $|i\rangle$ and $|j\rangle$, and their dependence on the grid size N.

i	j	N=10	N=20	N=40	N=80	N=200
0	1	0.0027494	0.0001120	0.0001130	0.0001130	0.0001130
0	2	0.2588751	0.7427083	0.7470755	0.7470755	0.7470755
0	3	0.0080954	0.0045662	0.0048149	0.0048149	0.0048149
0	4	0.0242874	0.0219536	0.0223187	0.0223187	0.0223187
0	5	0.0097093	0.0048293	0.0040180	0.0040180	0.0040180
1	2	0.0055681	0.0074483	0.0075479	0.0075479	0.0075479
1	3	0.7879808	0.7803590	0.7704241	0.7704241	0.7704241
1	4	0.0186331	0.0365620	0.0370082	0.0370082	0.0370082
1	5	0.0001858	0.0193159	0.0220963	0.0220963	0.0220963
2	3	0.0305122	0.3082355	0.3260697	0.3260697	0.3260697
2	4	0.4219174	1.2260224	1.3183019	1.3183019	1.3183019
2	5	0.0082896	0.3018197	0.2869016	0.2869016	0.2869016
3	4	0.4932864	1.9754476	1.9696534	1.9696534	1.9696534
3	5	0.0014546	0.6127348	0.6367535	0.6367535	0.6367535
4	5	0.0163778	5.6393118	5.6830635	5.6830635	5.6830635

TABLE 2: Numerical values of the transition moment $|\langle i|\mu|j\rangle|^2$ in 10^{-4} Å$^2e^2$, and their dependence on the grid size N.

We take the ground state $|0\rangle$ as the initial state ("reactant"). The goal of the control is to move the population into the other well ("product"). A technical problem in designing the control field by Eqs.(15) and (16) is that the initial condition $|\psi(0)\rangle = |0\rangle$ and $F(0) = 0$ is a stationary solution of Eqs. (15) and (16) and no time evolution can be obtained from this initial condition. We therefore make a small deviation from the pure ground state in the initial condition:

$$|\psi(0)\rangle = \sqrt{0.999}|0\rangle + \sqrt{0.001}|2\rangle. \tag{20}$$

The system then goes increasingly further from the initial state under the time propagation by Eqs. (15) and (16). After the field is obtained in this way, we perform a numerical simulation of the time evolution starting with the pure ground state $|\psi(0)\rangle = |0\rangle$ as the initial condition under the effect of the obtained field. In what follows, we plot the time evolution of the wavefunctions obtained in the latter time propagation calculation.

Figure 4 shows the results of calculation presented in the previous section, where we have put the parameter $\alpha = 1000$ a. u. Panel (a) shows the electric field obtained by the time propagation given by Eqs. (15) and (16). Panel (b) shows the time evolution of the population in each eigenstate, that is, $|\langle n|\psi(t)\rangle|^2$, for n = 0-5, under the effect of the electric field shown in (a). Populations for the higher states (n > 5) were found to be minor. The electric field is effective in the time range t < 20 ps. After the pulse, the system is successfully populated in the right well (the state $|1\rangle$) with more than 95% population. Since the present algorithm is constructed by the qualitative physical interpretation of the phase space structure, we consider that the success of the method in the control gives further support to our "catch-and-release" interpretation suggested in the previous work.[20]

For further analysis of the obtained field in Fig. 4 (a), we take a window Fourier transform defined by

$$S(\omega, t) \stackrel{\text{def}}{=} \left| \int_{t-T/2}^{t+T/2} w(t'-t)F(t')\exp(-\mathrm{i}\omega t')\mathrm{d}t' \right|^2, \tag{21}$$

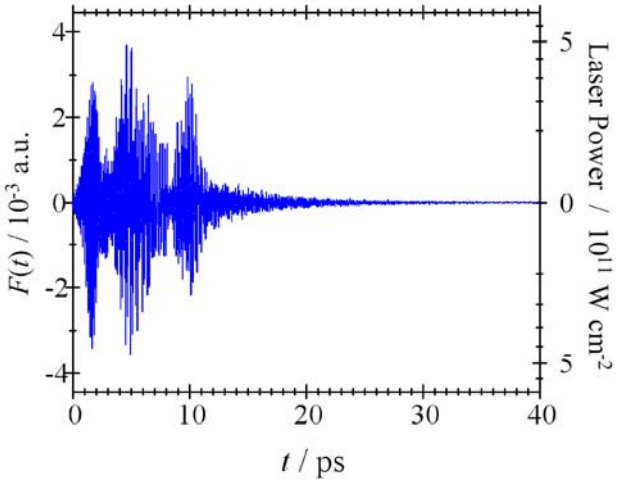
where w is a window function. The window Fourier transform gives the local power spectrum in the time range $[t - T/2, t + T/2]$. Here we take the window size T = 4.096 ps and the Blackman window

$$w(\tau) = 0.42 + 0.50\cos\left(\frac{2\pi\tau}{T}\right) + 0.08\cos\left(\frac{4\pi\tau}{T}\right).$$

(22)

The qualitative result did not change by replacing the window function to the rectangular and the Hanning windows.[51] Figure 5 shows the time-resolved power spectrum $S(\omega, t)$ of the field shown in Fig. 4 (a). We can find the frequency components corresponding to the transition sequence $|0\rangle \rightarrow |2\rangle \rightarrow |5\rangle \rightarrow |3\rangle \rightarrow |1\rangle$ as could already be seen by Fig. 4 (b). Note that the similar time-resolved power spectrum has been found for the local control field,[14] except that there the cost functional has been designed to make the system pass through the less excited state $|4\rangle$ instead of $|5\rangle$. The field obtained by the present method may not be a fully optimized one in that it uses the excited state $|5\rangle$ rather than $|4\rangle$. We will come back to this point in Summary and Outlook section.

(a)



(b)

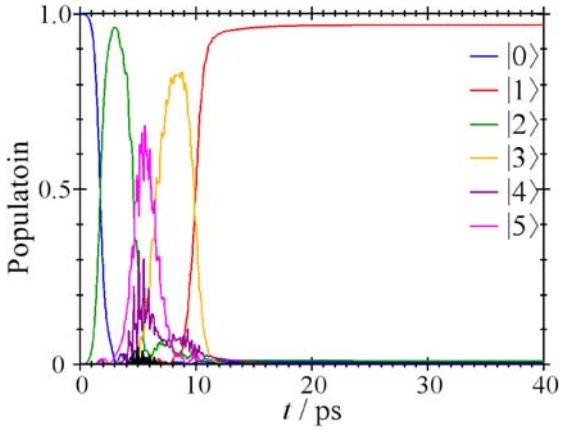


Fig. 4 Results of the control calculation with the field strength parameter $\alpha = 1000$ a.u. (a) The electric field. (b) Time evolution of the populations in the eigenstates.

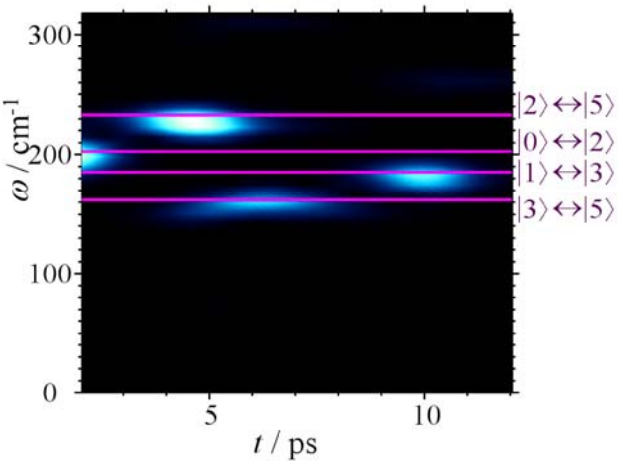
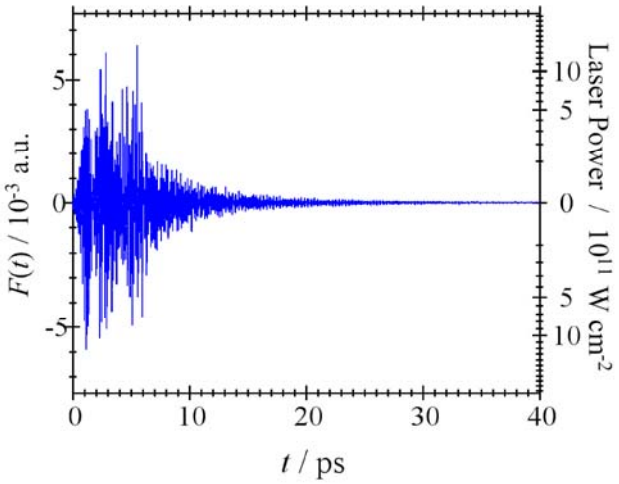


Fig. 5 Time-resolved power spectrum of the field shown in Fig. 4 (a). Light colors correspond to higher power. The relevant transition frequencies of the system are indicated by straight lines.

In the present procedure, the system is first excited by a small amount into the state $|2\rangle$ by a perturbation. Then, the system starts to oscillate due to the quantum beating between $|0\rangle$ and $|2\rangle$. As shown in Fig. 2, the present control algorithm makes the electric field change in accordance with the average position of the system. The reactivity boundary should approach the system in the reactant region only when the system is heading toward the barrier [Fig. 2 (b)]. Thus the field starts to oscillate with the same frequency with the system, and this oscillating field excites the system further. After the excitation, the system goes over the barrier through the state $|5\rangle$, and then it is de-excited in the product well $|3\rangle\rightarrow|1\rangle$, whence the system ceases its oscillation and the field decays to zero as well. The last part may need explanation since the state $|3\rangle$ is already in "product side" but the present method further de-excites the system into $|1\rangle$. This can be understood by noting that, when the system is on the product side [Fig. 2(d)], the present algorithm designs the field such that the reactivity boundary is as far from the system as possible. Therefore, even if the system is already on the product side, Eq. (15) still makes nonzero electric field according to the oscillation of the system in the product well: when the system is heading toward the reactant side, the reactivity boundary moves back slightly toward the reactant side to avoid the system. This field de-excites the system into the state $|1\rangle$ which is in the product region and "furthest" from the boundary.

(a)



(b)

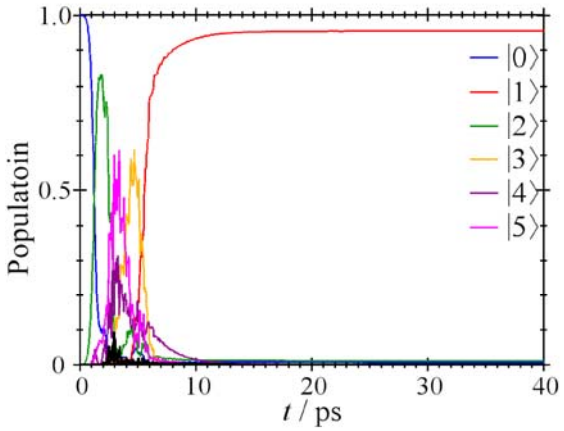
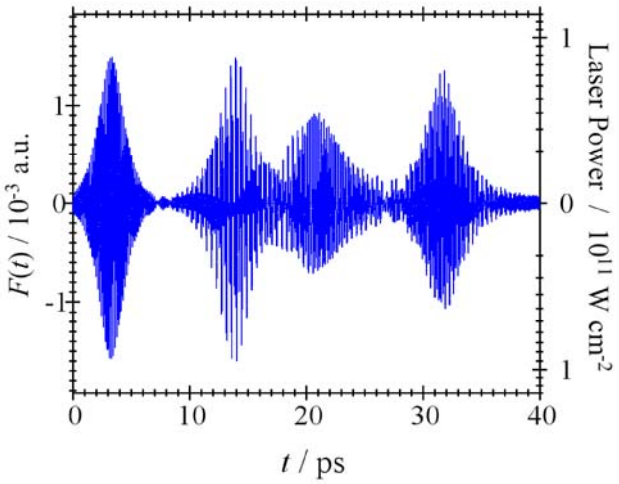


Fig. 6 Same as Fig. 4 but with the field strength parameter $\alpha = 1500$ a. u.

(a)



(b)

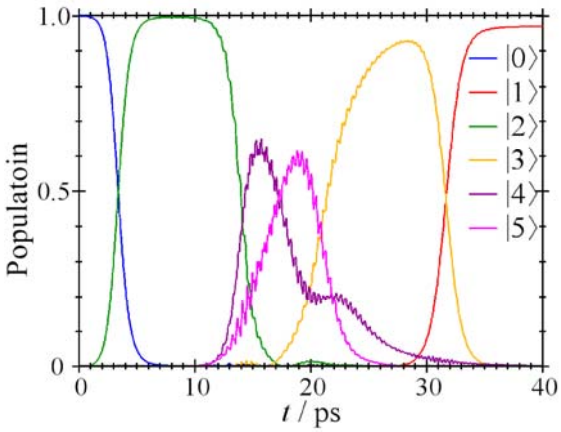


Fig. 7 Same as Fig. 4 but with the field strength parameter $\alpha = 500$ a. u.

Next we investigate the effect of the parameter α appearing in the present algorithm, since the choice of its value is somewhat arbitrary. Figure 6 shows the results obtained by setting $\alpha = 1500$ a. u., larger than the previous result. It is seen that the field is now stronger than the previous case, which is natural since the parameter α scales the field amplitude in Eq. (15). With this stronger field, the system reaches the target state in a shorter time [compare Fig. 4(b) and 6(b)]. It is well known, and mathematically stated in Ref. 15, that the control field is far from unique. There is actually infinite number of pulse shapes that can lead to the same target state. Analysis of the Hessian matrix of the cost functional[15] has shown that at the optimal solution for an N-level system, the cost functional is minimum only along N^2 directions in the space of $F(t)$, while along the other directions the landscape of the cost functional is flat (with zero curvature). Changing the pulse shape along these directions does not (at least to the quadratic approximation around the minimum) affect the optimality of the field. The freedom of the parameter α here, roughly corresponding to the time taken for reaching the target state, can represent one of such directions.

Quite naturally, the opposite behavior is observed when we decrease α. Figure 7 shows the results obtained by setting $\alpha = 500$ a. u. As expected, the field is weaker than the previous figures and guides the system to the target state more slowly.

Summary and Outlook

A procedure for designing a laser pulse to control chemical reactions was suggested on the basis of the physical interpretation found in the previous work. The method consists of a simultaneous solution of the time propagation of the wavefunction and an equation to determine the electric field. The latter equation conditions the electric field in such a way that the phase space reactivity boundary shifts toward the reactant side to catch the population located in the reactant region, and then guides the system toward the product side where it is released. The success of this method in controlling the reaction, demonstrated here with a model system, supports the validity of the physical interpretation of the control process by the "catch-and-release" mechanism.

The procedure constructed in the present work needs only a single simultaneous propagation of the system and the field. In this sense it belongs to the category of the local OCT.[14] However, it is still questionable whether this procedure is any better as a method than existing ones in the sense of optimality in the laser field design. In the global OCT, the concept of optimality depends on the definition of the cost functional. The latter includes, for example, a penalty factor for the field intensity and frequency constraints, whose choice is quite arbitrary.

Each choice of the cost function results in a distinct "optimal" field. To get the optimal field for each particular choice of the cost functional, it is best to use the global OCT to numerically optimize the full details of the pulse shape for that particular cost functional. The pulse shape obtained by the present method should not be optimal for all the different choices of the cost functional. Rather, our emphasis lies in obtaining physical insights in the control process. The success of the present procedure in guiding the system into the reaction product strengthens the validity of the "catch-and-release" concept. It can nevertheless be said that the present method, being a local OCT, has an advantage of requiring less computational power, and it may also serve to give a good initial guess of the pulse shape for the global OCT, since the latter is an iterative procedure which needs an initial guess.

APPENDIX A: DERIVATION OF EQ. (15)

By differentiating Eq. (10) with respect to *t*, we obtain

$$\frac{\mathrm{d}}{\mathrm{d}t}x^{\ddagger}(t) = \lambda x^{\ddagger}(t) - \frac{1}{\sqrt{2\lambda}}\mu_1 F(t),$$
$$\frac{\mathrm{d}}{\mathrm{d}t}\xi^{\ddagger}(t) = -\lambda \xi^{\ddagger}(t) - \frac{1}{\sqrt{2\lambda}}\mu_1 F(t). \tag{A1}$$

This simply says that Eq. (10) is a particular solution of Eq. (9). Differentiating Eq. (13) with respect to *t* and inserting Eq. (A1), we obtain

$$\frac{\mathrm{d}}{\mathrm{d}t}q^{\ddagger}(t) = \frac{1}{\sqrt{2\lambda}}\Big(\lambda x^{\ddagger}(t) + \lambda \xi^{\ddagger}(t)\Big). \tag{A2}$$

Differentiating once more and using Eq. (A1) again, we obtain

$$\frac{\mathrm{d}^2}{\mathrm{d}t^2}q^{\ddagger}(t) = \frac{1}{\sqrt{2\lambda}}\Big(\lambda^2 x^{\ddagger}(t) - \lambda^2 \xi^{\ddagger}(t) - \sqrt{2\lambda}\mu_1 F(t)\Big)$$
$$= \lambda^2 q^{\ddagger}(t) - \mu_1 F(t). \tag{A3}$$

One could have obtained Eq. (A3) more easily: Since $q^{\ddagger}$ is a particular solution of the equation of motion, Eq. (A3) is just the equation of motion given by the Hamiltonian of Eq. (7). From Eq. (A3) we can express the electric field in terms of $q^{\ddagger}$

$$F(t) = \frac{1}{\mu}\left(\lambda^2 - \frac{\mathrm{d}^2}{\mathrm{d}t^2}\right)q^{\ddagger}(t).$$

(A4)

Substituting Eq. (14) into Eq. (A4) gives Eq. (15).

ACKNOWLEDGMENTS

This work has been supported by Research Fellowships of the Japan Society for the Promotion of Science for Young Scientists (to SK) and by JSPS, JST/CREST, Priority Area 'Molecular Theory for Real Systems' (to TK). The computations were partially performed using the Research Center for Computational Science, Okazaki, Japan. We thank Professor Michihiko Sugawara in Keio University and Professor Tsuyoshi Kato in University of Tokyo for their instructive comments on the model system. Helpful comments from the reviewers are also acknowledged.

---

1. K. Yamanouchi, *Science* **2002**, *295*, 1659.
2. S. A. Rice and M. Zhao, *Optical Control of Molecular Dynamics* (Wiley, New York, **2000**).
3. M. Shapiro and P. Brumer, *Phys. Rep.* **2006**, *425*, 195.
4. T. Brabec and F. Krausz, *Rev. Mod. Phys.* **2000**, *72*, 545.
5. A. D. Bandrauk, ed., *Molecules in Laser Fields* (Marcel Dekker, New York, **1994**).
6. R. Kosloff, S. A. Rice, P. Gaspard, S. Tersigni, and D. J. Tannor, *Chem. Phys.* **1989**, *139*, 201.
7. W. Zhu, J. Botina, and H. Rabitz, *J. Chem. Phys.* **1998**, *108*, 1953.
8. W. Zhu and H. Rabitz, *J. Chem. Phys.* **1998**, *109*, 385.
9. R. S. Judson and H. Rabitz, *Phys. Rev. Lett.* **1992**, *68*, 1500.
10. K. Sundermann and R. de Vivie-Riedle, *J. Chem. Phys.* **1999**, *110*, 1896.
11. J. Werschnik and E. K. U. Gross, *J. Opt. B* **2005**, *7*, S300.
12. J. Werschnik and E. K. U. Gross, *J. Phys. B* **2007**, *40*, R175.
13. M. Lapert, R. Tehini, G. Turinici, and D. Sugny, *Phys. Rev. A* **2009**, *79*, 063411.
14. M. Sugawara and Y. Fujimura, *J. Chem. Phys.* **1994**, *100*, 5646.
15. T.-S. Ho, J. Dominy, and H. Rabitz, *Phys. Rev. A* **2009**, *79*, 013422.
16. R. J. Levis, G. M. Menkir, and H. Rabitz, *Science* **2001**, *292*, 709).
17. C. Daniel, J. Full, L. González, C. Lupulescu, J. Manz, S. V. A. Merli, and L. Wöste,

Science **2003**, *299*, 536.

18. B. J. Sussman, D. Townsend, M. Y. Ivanov, and A. Stolow, *Science* **2006**, *314*, 278.
19. S. Kawai, A. D. Bandrauk, C. Jaffé, T. Bartsch, J. Palacián, and T. Uzer, *J. Chem. Phys.* **2007**, *126*, 164306.
20. S. Kawai and T. Komatsuzaki, *J. Chem. Phys.* **2011**, *134*, 024317.
21. *Geometric Structures of Phase Space in Multidimensional Chaos: Applications to Chemical Reaction Dynamics in Complex Systems* in *Advances in Chemical Physics*, ed. by M. Toda, T. Komatsuzaki, T. Konishi, R. S. Berry, S. A. Rice, John-Wiley & Sons, Inc., **2005**, Vol. 130, doi:10.1002/0471712531, and references therein.
22. *Advancing Theory for Kinetics and Dynamics of Complex, Many-Dimensional Systems: Clusters and Proteins* in *Advances in Chemical Physics*, ed. by T. Komatsuzaki, R. S. Berry, D. M. Leitner, John-Wiley & Sons, Inc., **2011**, Vol. 145. doi:10.1002/9781118087817.
23. R. Hernandez and W. H. Miller, *Chem. Phys. Lett.* **1993**, *214*, 129.
24. R. Hernandez, *J. Chem. Phys.* **1994**, *101*, 9534.
25. T. Komatsuzaki and R. S. Berry, *J. Chem. Phys.* **1999**, *110*, 9160.
26. T. Komatsuzaki and R. S. Berry, *Proc. Nat. Acad. Sci. USA* **2001**, *98*, 7666.
27. S. Wiggins, L. Wiesenfeld, C. Jaffé, and T. Uzer, *Phys. Rev. Lett.* **2001**, *86*, 5478.
28. T. Uzer, C. Jaffé, J. Palacián, P. Yanguas, and S. Wiggins, *Nonlinearity* **2002**, *15*, 957.
29. T. Komatsuzaki, R. S. Berry, *Chemical Reaction Dynamics: Many-Body Chaos and Regularity* in *Advances in Chemical Physics*, ed. by I. Prigogine, S. A. Rice, John Wiley & Sons, Inc., **2003**, Vol. 123, Chap. 2, pp. 79-152. doi:10.1002/0471231509.ch2.
30. S. Kawai, H. Teramoto, C.-B. Li, T. Komatsuzaki, M. Toda, in *Advancing Theory for Kinetics and Dynamics of Complex, Many-Dimensional Systems: Clusters and Proteins* in *Advances in Chemical Physics*, ed. by T.Komatsuzaki, R. S. Berry, D. M. Leitner, John-Wiley & Sons, Inc., **2011**, Vol. 145, Chap. 4, pp. 123-169. doi:10.1002/9781118087817.ch4.
31. C.-B. Li, A. Shojiguchi, M. Toda, and T. Komatsuzaki, *Few-Body Systems* **2006**, *38*, 173.
32. C.-B. Li, A. Shojiguchi, M. Toda, and T. Komatsuzaki, *Phys. Rev. Lett.* **2006**, *97*, 028302.
33. T. Bartsch, R. Hernandez, and T. Uzer, *Phys. Rev. Lett.* **2005**, *95*, 058301.
34. T. Bartsch, T. Uzer, and R. Hernandez, *J. Chem. Phys.* **2005**, *123*, 204102.
35. T. Bartsch, T. Uzer, J. M. Moix, and R. Hernandez, *J. Chem. Phys.* **2006**, *124*, 244310.
36. T. Bartsch, *J. Chem. Phys.* **2009**, *131*, 124121.
37. R. Hernandez, T. Uzer, and T. Bartsch, *Chem. Phys.* **2010**, *370*, 270.

38. T. Bartsch, J. M. Moix, R. Hernandez, S. Kawai, T. Uzer, *Time-Dependent Transition State Theory* in *Advances in Chemical Physics*, ed. by S. A. Rice, John Wiley & Sons, Inc., **2008** , Vol. 140, Chap. 4, pp. 191-238. doi:10.1002/9780470371572.ch4.
39. S. Kawai and T. Komatsuzaki, *J. Chem. Phys.* **2009**, *131*, 224505.
40. S. Kawai and T. Komatsuzaki, *J. Chem. Phys.* **2009**, *131*, 224506.
41. S. Kawai and T. Komatsuzaki, *Phys. Chem. Chem. Phys.* **2010**, *12*, 7626.
42. S. Kawai and T. Komatsuzaki, *Phys. Chem. Chem. Phys.* **2010**, *12*, 7636.
43. S. Kawai and T. Komatsuzaki, *Phys. Chem. Chem. Phys.* **2010**, *12*, 15382.
44. S. Kawai and T. Komatsuzaki, *Phys. Rev. Lett.* **2010**, *105*, 048304.
45. H. Waalkens, R. Schubert, and S. Wiggins, *Nonlinearity* **2008**, *21*, R1.
46. A. Goussev, R. Schubert, H. Waalkens, and S. Wiggins, *J. Chem. Phys.* **2009**, *131*, 144103.
47. L. E. Fried and G. S. Ezra, *J. Phys. Chem.* **1988**, *92*, 3144.
48. *Quantum Mechanics in Phase Space*, C. K. Zachos, D. B. Fairlie, and T. L. Curtright, World Scientific Publishing, Singapore, **2005**.
49. *Density-Functional Theory of Atoms and Molecules*, R. G. Parr and W. Yang, Oxford University Press, New York, **1989**.
50. D. T. Colbert and W. H. Miller, *J. Chem. Phys.* **1992**, *96*, 1982.
51. *Numerical Recipes in C*, W. H. Press, S. A. Teukolsky, W. T. Vetterling, and B. P. Flannery, Cambridge University Press, Cambridge, **1992**